Supplementary Information for

Ultrafast Floquet engineering of Fermi-polaron resonances in charge-tunable monolayer WSe_2 devices

Hyojin Choi[1,2,†], Jinjae Kim[1,2,†], Jiwon Park[1.2], Jekwan Lee[1,2], Wonhyeok Heo[3], Jaehyeon Kwon[3], Suk-Ho Lee[4,5], Faisal Ahmed[6], Kenji Watanabe[7], Takashi Taniguchi[7], Zhipei Sun[6], Moon-Ho Jo[4,5,*], and Hyunyong Choi[1,2,*]

[1] Department of Physics and Astronomy, Seoul National University, Seoul 08826, Korea

[2] Institute of Applied Physics, Seoul National University, Seoul 08826, Korea

[3] Semiconductor R&D Center, Samsung Electronics, Suwon 18848, Korea

[4] Department of Materials Science and Engineering, Pohang University of Science and Technology, Pohang 37673, Korea.

[5] Center for van der Waals Quantum Solids, Institute for Basic Science (IBS), Pohang 37673, Korea.

[6] Department of Electronics and Nanoengineering, Quantum Technology Finland Centre of Excellence, Aalto University, Tietotie 3, FI-02150, Espoo, Finland

[7] Advanced Materials Laboratory, National Institute for Materials Science, 1-1 Namiki Tsukuba 305-0044, Japan

[†]These authors contributed equally: Hyojin Choi, Jinjae Kim

[*]Corresponding author: mhjo@postech.ac.kr, hy.choi@snu.ac.kr

Content

Supplementary Notes

1. Reflectance contrast spectroscopy in an electron-doped regime

We conduct the additional steady-state RC measurements with varying the Fermi energy in an electron-doped regime, $E_{\mathrm{F,e}}$ up to 18 meV. In the electron-doped regime, two attractive polarons emerge at photon energy of 1.6851 eV and 1.6917 eV, as depicted in Supplementary Fig. 1a. This additional splitting of attractive polarons is not seen in the hope-doped regime. Supplementary Fig. 1b shows three resonances, corresponding to two attractive polarons and one repulsive polaron when $E_{\mathrm{F,e}}$ is 6.7 meV. Because the spin-orbit coupling of conduction band (~38 meV) is much smaller than the valence band (~400 meV)[1], we consider the low-energy scattering states in which two opposite spin states of electrons are in the same valley (singlet polaron) and in the different valleys (triplet polaron). Such configurations are illustrated in Supplementary Fig. 1c. The energetically lower state corresponds to an intravalley singlet polaron, in which an exciton and the interacting Fermi sea are in the same valley, and the higher energy state is an intervalley triplet polaron, where an exciton and the Fermi sea are located in different valleys. In the case of the intravalley singlet polaron, the electron of an exciton and the Fermi sea are in different spin states due to the Pauli exclusion principle. As a result, the electron resides in the upper conduction band while the excess electrons are located in the lower conduction band within the same valley, forming a singlet polaron. For the intervalley polaron, the electron of an exciton and the excess electrons have different valley indices but occupy the same spin state, resulting in the formation of a triplet polaron[2]. For both cases, the optical selection rule dictates that the electrons of excitons are located in the higher conduction band, while the excess electrons reside in the lower conduction band.

Indeed, a closer inspection of Supplementary Figs. 1a and 1b reveals that there is an

additional fine structure splitting (~7 meV) whose origin can be understood by considering the exchange interaction. The exchange interaction necessitates a finite spatial distance between the Fermi sea and the hole of the exciton when they occupy the same spin state. As a result, the energy level of the triplet polaron is increased, leading to the higher resonance for the triplet polaron and the lower resonance for the singlet polaron. The energy difference for WSe_2 is calculated to be approximately 6 meV[3], which agrees well with our measured splitting of 7 meV.

Although the singlet and triplet splitting is interesting, there are the following reasons why we have focused on the experiments in the hole-doped regime in monolayer WSe_2. First, the two branches of attractive polarons (in the electron-doped regime) are too closely spaced in the spectral domain, as mentioned in the above paragraph. Because of the small energy difference (about 7 meV) between the two attractive polaron resonances, there is a significant overlap between the two polaron spectra, making it difficult to clearly resolve the singlet and triplet polarons (see Supplementary Figs. 1d and 1e). Supplementary Fig. 1b presents the reflectance contrast at $E_{\mathrm{F,e}} = 6.7$ meV, while Supplementary Fig. 1f displays the corresponding the below-gap pump-induced reflectance contrast at the same $E_{\mathrm{F,e}}$. Because the overlap of the transient spectrum from the two attractive polaron resonances is significant, it is challenging to extract the shift of each attractive polaron energy accurately. In contrast, as schematically shown in Supplementary Fig. 1g, only one attractive polaron is formed in the hole-doped regime.

Secondly, for the choice of the molybdenum-based materials, the energy difference between the upper and lower conduction band is much smaller, compared to the tungsten-based materials. For example, MoS_2 shows a difference of only 3 meV and $MoSe_2$ of 21 meV, whereas WS_2 and WSe_2 exhibit a difference of 27 meV and 38 meV, respectively[1]. Given these

differences, the molybdenum-based materials might not reveal the distinct spectral characteristics of the Fermi polarons. Meanwhile, in the monolayer WSe_2, the valence band exhibits a spin-orbit coupling (~500 meV) an order of magnitude larger than that of the conduction band. This significant difference in spin-orbit coupling is the primary reason we focus on the hole-doped regime.

2. Spectra analysis of attractive and repulsive polarons in a hole-doped regime

We conduct the optical spectroscopy in a reflection geometry on an additional gate-tunable WSe_2 monolayer device with changing the hole density n_h. An optical microscopy image of another device is shown in Supplementary Fig. 2a. Supplementary Figs. 2b and 2c show the reflectance contrast (RC) measured with varying $E_{F,h}$ from 0 meV to -28.6 meV. The repulsive polaron branch exhibits a blue shift towards a higher photon energy and experiences a significant increase of linewidth as $E_{F,h}$ increases. In contrast, the attractive polaron resonance shows a slight red shift towards a lower photon energy with a relatively small broadening of the linewidth.

For more details on the linewidth broadening, Supplementary Fig. 2d indicates a significant increase in the linewidth of the repulsive polarons from 10.6 meV to 55.4 meV with increasing $E_{F,h}$ toward more hole doping, while the linewidth of the attractive polarons exhibits a minor increase from 7.1 meV to 12.5 meV. The large change in the linewidth of the repulsive polarons resembles the homogeneously broadened linewidth, as observed in prior reports[4,5]. Recent measurements using four-wave-mixing spectroscopy have reported the details on the kinetics of the linewidth broadening, denoted as 2γ, where γ represents the decoherence rate. This rate is inversely proportional to the dephasing time (T), defined as $\frac{\gamma}{\hbar} = \frac{1}{T}$[6]. The increased linewidth of the repulsive polarons necessitates an additional $E_{F,h}$-dependent damping term, related to the non-radiative transitions from the repulsive polarons to the attractive polarons. When the excess holes in the Fermi sea and the exciton are in the different valleys, the excitons are polaronically dressed without the Pauli blocking effects. With increasing $E_{F,h}$, the decay rate significantly increases. Such an additional broadening (γ_{add}) in the repulsive polarons can be calculated using the Fermi's golden rule as $\gamma_{add} \approx \frac{3\pi M^2}{4}\frac{E_F^2 \Delta E_X}{\Delta E_T^2}$[7], where ΔE_X is the binding energy of excitons, the dimensionless constant M is the overlap

between polaronic dressing of the initial state and the final state of the repulsive polarons, and ΔE_{T} is the binding energy of trions.

The resonance shifts of the repulsive and attractive polarons exhibit distinct features with varying $E_{\mathrm{F,h}}$. The increase in the carrier density induces several effects, such as bandgap renormalization, Pauli blocking, and carrier-induced screening. Supplementary Fig. 2e shows that the resonance peak energy of the repulsive polarons (black squares) is blueshifted, while that of the attractive polarons (red circles) is redshifted. These effects also lead to the enhanced (reduced) oscillator strength in the attractive (repulsive) polarons. In calculating the oscillator strength of Fermi polarons, we conduct an integration of the amplitude over the region around the attractive and the repulsive polaron resonance in the RC spectra[8]. The repulsive polarons, which are considered to be the unbound quasiparticles of excitons with surrounding Fermi sea, experience the Pauli blocking effect and the Coulomb screening between the electrons and the holes in the excitons. The increased Pauli blocking effects result in a reduction in the exciton binding energy. The itinerant holes induce the attenuation of the electric fields, which causes a decrease in the attractive Coulomb interaction. The screening of the attractive interactions between the electrons and the holes lowers the exciton binding energy. The reduced exciton binding energy results in the blueshift and the reduction of the oscillator strength of the repulsive polarons (black squares)[9,10].

For the attractive polarons (red circles in Supplementary Fig. 2e), the resonance is redshifted. It is a prominent characteristic of the attractive polaron formation that distinguishes it from trions. If one assumes a trion model, the trion binding energy should decrease with increasing carrier density due to the Pauli blocking effects and the Coulomb screening. Meanwhile, the exciton-polaron theory suggests that the attractive interactions between the excitons and the itinerant Fermi sea are enhanced when more free carriers are introduced[11]. An increase in attractive interactions leads to a stronger binding energy of the attractive polarons,

which resulting in the redshift of the attractive polarons and the enhanced oscillator strength (red circles).

3. Ultrafast pump-probe spectroscopy under 3.1 eV pump excitation

The energy shift of Fermi polarons arises spontaneously due to off-resonant pump excitation, and the temporal transients are characterized by the short-lived signals. To demonstrate that our data in the main section do not arise from any real carriers from the above gap (e.g. two-photon absorption or band-to-band carrier excitation), we perform the absorption pump-probe spectroscopy with two distinct pump energy; one below the optical band-gap and one above electronic band-gap (see Supplementary Fig. 3a and 3b, respectively). We adjust $E_{\mathrm{F,h}}$ at three specific points. All spectra are obtained using pump and probe pulses with the same circular polarization. The pump-pulse energy in Supplementary Fig. 3a is 1.55 eV, while it is 3.1 eV in Supplementary Fig. 3b.

The attractive polarons emerge regardless of the pump energy, as shown in Supplementary Fig. 3b. The main difference is in the temporal dynamics. The above-gap excitation leads to the generation of highly energetic carriers, which then proceed to relax by multiple relaxation pathways. The relaxation times of the attractive polarons are measured to be 2.68 ps and 2.51 ps at $E_{\mathrm{F,h}}$ of -12.7 meV and -27.9 meV, respectively. The relaxation time becomes short with increasing the carrier density. These observations can be explained by considering the interactions between the attractive polarons and the free carriers. Upon initial injection of holes, the carriers promote the production of the attractive polarons, and enhance the attractive polaron absorption. However, with increasing the carrier density, free carriers scatter with the attractive polarons, resulting in the reduced relaxation times[12]. For the repulsive polarons, we have measured 3.57 ps and 1.07 ps at $E_{\mathrm{F,h}}$ of 0 meV and -12.7 meV. The relaxation time also decreases because of the same reasons of the attractive polarons.

The two-dimensional plot depicted in Supplementary Fig. 3a exhibit clear differences compared to the signals shown in Supplementary Fig. 3b. The signals shown in Supplementary

Fig. 3a quickly diminish for the pump-probe time delay over 300 fs, whereas the signals for the Fermi polarons last for 1.07~3.57 ps. Additionally, there is no change in energy levels of the resonances in Supplementary Fig. 3b. These results demonstrate that the resonance shifts of the Fermi polarons discussed in the main section are distinct from those with the above-gap excitation.

4. Discussions on the fit functions

We have used different oscillator models to describe the reflectance contrast spectrum and the pump-induced changes in the reflectance contrast. For the "steady-state" reflectance contrast measurements, we employ a Lorentzian oscillator model. However, when fitting the pump-probe spectroscopy results, we utilize a Gaussian oscillator. The reason behind this choice is based on the distinct characteristics of Lorentzian and Gaussian oscillators. Lorentzian oscillators are typically used to describe homogeneous broadening, which is due to intrinsic properties such as radiative lifetimes or collision effects. On the other hand, Gaussian oscillators are better suited for inhomogeneous broadening, where the width includes effects of either spatial or spectral variations. In our "steady-state" reflection contrast measurements, we use a stable continuous-wave (c.w.) laser. Under these conditions, fitting with the Lorentzian oscillator model is more appropriate. However, under the off-resonant pump excitation, we have measured the ensemble averages of both spatial and spectral species, making a Gaussian oscillator more suitable. Gaussian fits are less sensitive to noise compared to Lorentzian fits because Gaussian profiles have smoother tails on the spectral wings. This makes the fitting process more robust in the presence of noise.

For the "isolated" exciton resonance shift, the resonance shifts including the Stark shift may be fitted using either the integral of the change of absorption from the experimental data[13] or by taking the derivative of the absorption spectra[14]. Assuming a Gaussian lineshape of the absorption spectrum, the corresponding energy shift ΔE can be mathematically represented as $\alpha(\omega, \Delta E) = \mathrm{A}\exp(-\frac{(\omega-\Delta E)^2}{2c^2})$, where A represents the absorption peak and c indicates the full width of half maximum divided by $2\sqrt{2\,ln2}$. The value of $\Delta\alpha(\omega, \Delta E)$, obtained through the pump-probe experimental data, can be calculated as $-\frac{\partial\alpha}{\partial\omega}\Delta E$. Hence, many literatures have

used the derivatives of the absorption spectra to analyze the resonance shift. Because $-\frac{\partial\alpha}{\partial\omega}\Delta E$ is $\frac{\omega}{c^2}\alpha(\omega)\Delta E$, one may calculate the transient energy shift of a single resonance by integrating the area under $\Delta\alpha(\omega,\Delta E)$, which is represented as $\int_0^\infty \Delta\alpha(\omega,\Delta E)d\omega = A\Delta E$. One assumption of these approaches is that the involved resonance is "isolated" from the environment, with no consideration of the Fermi sea.

Whereas these techniques are applicable for determining the Stark shift of a single oscillator, but they are not useful for estimating the resonance shifts if two or more oscillators are present. In fact, integrating the experimental data or taking the derivative of the absorption spectra pose a mathematical restriction that the measured $\Delta R/R_0$ should exhibit a symmetric lineshape. Due to the small energy difference between the attractive and the repulsive resonances, a significant spectral overlap occurs in our case. Of course, Fig. 2c in the main text shows the experimental results of the symmetric lineshape when $E_{\mathrm{F,h}}$ is 0 meV. Meanwhile, the experimental data at $E_{\mathrm{F,h}}$ of -12.4 meV (Fig. 2d in the main text) indicates asymmetric lineshapes for both the attractive and repulsive polaron resonance. Consequently, we fit the measured $\Delta R/R_0$ spectrum with using a Gaussian shifting method to extract the resonance shifts from the experimental data. The change in absorbance can be calculated with using the following Gaussian function[15-17],

$$\Delta\alpha(\omega) = A_{\mathrm{A}}\exp\left(-\frac{(\omega-E_{\mathrm{A}})^2}{2c_{\mathrm{A}}^2}\right) - A_{\mathrm{A}}\exp\left(-\frac{(\omega-E_{\mathrm{A}}-\Delta E_{\mathrm{A}})^2}{2c_{\mathrm{A}}^2}\right)$$

$$+A_{\mathrm{R}}\exp\left(-\frac{(\omega-E_{\mathrm{R}})^2}{2c_{\mathrm{R}}^2}\right) - A_{\mathrm{R}}\exp\left(-\frac{(\omega-E_{\mathrm{R}}-\Delta E_R)^2}{2c_{\mathrm{R}}^2}\right), \qquad \text{(S1)}$$

where A_{A}, E_{A}, c_{A}, ΔE_{R}, A_{R}, E_{R}, c_{R} and ΔE_{R} refer to the absorption amplitude of the attractive polarons, the resonance energy of the attractive polarons, the full width of half

maximum divided by $2\sqrt{2\,ln2}$ of the attractive polarons, the energy shift of the attractive polarons, the absorption amplitude of the repulsive polarons, the resonance energy of the repulsive polarons, the full width of half maximum divided by $2\sqrt{2\,ln2}$ of the repulsive polarons and the energy shift of the repulsive polarons, respectively.

5. Pump-detuning dependence

Supplementary Figs. 4a, 4b and 4c show that the shift of Fermi polarons varies with the pump detuning. As the pump detuning decreases, the shift of the polarons increases. Such an inverse dependence on the pump detuning is well established and explained by the conventional dressed atom-photon pictures. However, we have realized that our data do not correspond to such models, indicating the need for a more elaborate model Hamiltonian. In Note 6, we have presented detailed discrepancies between the dressed atom-photon models and our measured data.

In contrast to non-interacting excitonic Stark effects, our case involves both the repulsive and attractive polarons, which arise from the interactions between the excitons and the surrounding Fermi sea. As discussed in the main text, the shift of the repulsive polarons follows the properties of excitons both in the steady state and under the off-resonant pump excitation. Consequently, the shift in the repulsive polarons would scale inversely with the pump-energy detuning, consistent with the conventional exciton optical Stark effect. However, the shift in the attractive polarons differs from that in the repulsive polarons. There is an additional blueshift in the attractive polarons compared to the repulsive polarons, resulting in a larger shift in the attractive polarons. We attribute this blueshift, which is absent in the repulsive polarons, to the decreased binding energy of the attractive polarons. Therefore, the shift in the attractive polarons can be interpreted as the sum of the shift from the conventional model and the shift due to the reduced binding energy. The shift due to the reduced binding energy in the attractive polarons is supposed to be independent of the pump detuning, caused by the hot carriers under off-resonant pump excitation. We assume that the number of hot carriers does not significantly change when the detuning is varied by 20 meV.

We consider that the attractive polaron shift is the sum of the shift from the conventional

model and the shift from the reduced binding energy. It means that the shift consists of a component that is inversely proportional to the pump detuning and another component that is independent of the detuning. This is supported by our measurements of the shift of Fermi polarons as a function of the pump detuning (see Supplementary Fig. 4). We measure the energy shifts of Fermi polarons at three different doping levels, $E_{\mathrm{F,h}} = 0$ meV, -8.6 meV, and -12.4 meV (Supplementary Figs. 4a, 4b and 4c). By extracting the energy shifts of the Fermi polarons from measurements, we see that the shifts decrease with increasing the detuning due to the change in Stark shifts. Additionally, we observe that the shift due to the reduced binding energy does not change with the pump detuning. This leads that the transient shift is rather "flat" regardless of the pump detuning. This argument is consistent with the expression for the shifts of Fermi polarons, $\Delta E_{\mathrm{P}} \cong 2\frac{M_{\mathrm{gx}}^2 \varepsilon^2}{E_{\mathrm{X}} - \hbar\omega_{\mathrm{pump}}} + \mathrm{constant}$ (gray dashed lines for the repulsive polarons and red dashed lines for the attractive polarons). Additionally, there might be a concern regarding the reference energy we should use for the pump detuning when $E_{\mathrm{F,h}} \neq 0$. In this case, we obtain the detuning by considering the energy level of the repulsive polarons. As discussed above, we have $\Delta E_{\mathrm{P}} \cong 2\frac{M_{\mathrm{gx}}^2 \varepsilon^2}{E_{\mathrm{X}} - \hbar\omega_{\mathrm{pump}}} + \mathrm{constant}$, so that determination of the detuning requires knowing the energy level of the excitons. In the finite hole-doped regime ($E_{\mathrm{F,h}} \neq 0$), because the attractive and repulsive polaron branches are present, it makes impossible to extract the energy level of the excitons. We note that although the general features of the repulsive polarons, such as decreased oscillator strength and the blue-shifted energy levels, are similar to those of excitons, the exciton characteristics also vary with changing the carrier density. Therefore, we use the energy level of the repulsive polarons to calculate the detuning instead of that of excitons.

6. Isolated atom-photon interaction model of the optical Stark effect

The conventional atom-photon model used to explain the optical Stark effect has proven insufficient in describing the resonance shift of Fermi polarons. In this Note, we provide a series of dressed atom-photon pictures, including two- and three-level model, and present why such models fail to account for the Fermi-polaron cases.

The optical Stark effect occurs because the virtual states experience a repulsion interaction with the equilibrium states. In the semi-classical theory, when optical pump field $h\omega_{\mathrm{pump}}$ is present, the ground state $|g\rangle$ and A-exciton $|x\rangle$ are hybridized, forming the Floquet quasistates $|g + \hbar\omega_{\mathrm{pump}}\rangle$ and $|x - \hbar\omega_{\mathrm{pump}}\rangle$ due to the light-matter coupling. As shown below, the conventional atom-photon interaction models (neither two-level nor three-level model) fail to explain our experimental observations.

In the simple two-level model, we can construct the effective Hamiltonian to calculate the energy shift for $|x\rangle$ as

$$H_{2-\mathrm{level}} = \begin{pmatrix} \hbar\omega_{\mathrm{pump}} & V_{\mathrm{X}} \\ V_{\mathrm{X}} & E_{\mathrm{A}} \end{pmatrix}, \tag{S2}$$

where $E_{|g\rangle} = 0$ and $E_{|x\rangle} = E_{\mathrm{A}}$, the energy level of A-exciton. V_{X} refers to the light-matter coupling, which can be described as $V_{\mathrm{X}} = M_{\mathrm{gx}}\varepsilon$, where ε is the amplitude of the applied electric field and M_{gx} is the polarization matrix element between $|g\rangle$ and $|x\rangle$[13]. With the same shift of the energy level for the ground state, the calculated energy level increases by $\Delta E \cong 2\frac{M_{\mathrm{gx}}^2\varepsilon^2}{E_{\mathrm{A}}-\hbar\omega_{\mathrm{pump}}}$, where the numerator M_{gx}^2 is proportional to the oscillator strength f_{osc}[18]. As shown in Fig. 1d in the main text, the oscillator strength of attractive polarons is significantly smaller than that of repulsive polarons. When using the two-level model, the energy shift Δ_{P} of attractive polarons should be much smaller than that of repulsive polarons,

as shown in the Supplementary Fig. 5a. However, our experiments demonstrate that Δ_{p} is larger for the attractive polarons compared to the repulsive polarons (Fig. 3b in the main text). Thus, we have found that such the two-level atom-photon interaction model does not reproduce the data when the excess charges exist. Notably, there is a significant discrepancy in Δ_{p} for attractive polarons between the results predicted by the two-level model and the experimental data.

Similarly, the three-level model that includes the ground state, the attractive polaron state, and the repulsive polaron state, is also found to be failed to capture the observed phenomena. To calculate the energy level shift of attractive and repulsive polarons caused by the Floquet quasistate, $|g + \hbar\omega_{\mathrm{pump}}\rangle$, we have constructed the following Hamiltonian under the assumption that there is no interaction between the attractive polarons and the repulsive polarons.

$$H_{3-\mathrm{level,p}} = \begin{pmatrix} \hbar\omega_{\mathrm{pump}} & V_{\mathrm{AP}} & V_{\mathrm{RP}} \\ V_{\mathrm{AP}} & E_{\mathrm{AP}} & 0 \\ V_{\mathrm{RP}} & 0 & E_{\mathrm{RP}} \end{pmatrix} \tag{S3}$$

Additionally, we consider the shift of the energy level for ground state with

$$H_{3-\mathrm{level,g}} = \begin{pmatrix} 0 & V_{\mathrm{AP}} & V_{\mathrm{RP}} \\ V_{\mathrm{AP}} & E_{\mathrm{AP}} - \hbar\omega_{\mathrm{pump}} & 0 \\ V_{\mathrm{RP}} & 0 & E_{\mathrm{RP}} - \hbar\omega_{\mathrm{pump}} \end{pmatrix}, \tag{S4}$$

where V_{AP} (V_{RP}) is the light-matter coupling between $|g\rangle$ and the attractive (repulsive) polaron state, which can be expressed as $V_{\mathrm{AP}} = M_{\mathrm{AP}}\varepsilon$ ($V_{\mathrm{RP}} = M_{\mathrm{RP}}\varepsilon$), where M_{AP} (M_{RP}) is the polarization matrix element between $|g\rangle$ and the attractive (repulsive) polaron state. The calculated Δ_{p} for the attractive polarons and the repulsive polarons with varying $E_{\mathrm{F,h}}$ is shown in the solid line in Supplementary Fig. 5b. The solid black line indicates Δ_{p} of the

repulsive polarons, and the solid red line represents Δ_p of the attractive polarons. Compared to the two-level model, Δ_p of attractive polarons becomes larger than the results predicted by the two-level model. However, it remains too small to reproduce the experimental data, which show that Δ_p of the attractive polarons is larger than that of the repulsive polarons. This discrepancy arises because when the Floquet quasistate $|g + \hbar\omega_{pump}\rangle$ shows the repulsion with the attractive polaron state, the repulsion is more significant with larger values of M_{AP}. However, since the attractive polarons have a smaller oscillator strength, the repulsion is weaker, resulting in a smaller shift for the attractive polarons.

To address these discrepancies, our next attempt is to consider another three-level model after including the interaction factor (γ) between the attractive and repulsive polarons[7].

$$H^*_{3-level,p} = \begin{pmatrix} \hbar\omega_{pump} & V_{AP} & V_{RP} \\ V_{AP} & E_{AP} & \gamma \\ V_{RP} & \gamma & E_{RP} \end{pmatrix}. \quad \text{(S5)}$$

However, this model results in a repulsion between the attractive and repulsive polaron states, causing the attractive polarons to redshift as shown in the dashed red line in Supplementary Fig. 5b. Due to the higher energy level of the repulsive polarons, the repulsive polarons shifts upwards, while the attractive polarons shift downwards. Consequently, this model also cannot reproduce the experimental data, where Δ_p of the attractive polarons is larger than that of the repulsive polarons.

7. More details on the polaron theory

We start here with a brief overview of the well-established *N*-body Green's function approach[19]. The retarded Green's function for a single impurity particle is defined by

$$iG_{ij}^{r}(t) = \Theta(t)\langle 0|\left[h_i(t),\, h_j^{\dagger}\right]|0\rangle\,, \tag{S6}$$

where the state vector $|0\rangle$ is the ground state of *N* fermions (holes) in the absence of impurity (exciton), h_i and $h_j^{\dagger}$ are the annihilation and creation operators of the i-th and j-th holes, respectively, and the prefactor $\Theta(t)$ is the Heaviside step function to meet the causality. The equation of motions in the Heisenberg picture is given by

$$i\partial_t A(t) = [A(t),\, H]\,, \tag{S7}$$

which leads to the equation of motion for the retarded Green's functions,

$$i\partial_t G_{ij}^{r}(t) = \delta(t)\langle 0|\left[h_i(t),\, h_j^{\dagger}\right]|0\rangle + G^{r}_{[h_i(t),\,H],\,j}(t). \tag{S8}$$

Taking the temporal Fourier transform with respect to t, we obtain

$$\omega G_{ij}^{r}(\omega) = \langle 0|\left[h_i,\, h_j^{\dagger}\right]|0\rangle + G^{r}_{[h_i(t),\,H],\,h_j^{\dagger}}(\omega). \tag{S9}$$

In the case of non-interacting free fermions (holes), we can obtain a closed expression for the Green's functions. We consider a Hamiltonian of the form

$$H = \textstyle\sum_k \epsilon_k h_k^{\dagger} h_k, \tag{S10}$$

where the eigenvalue ϵ_k depends on the dispersion of the system, specifically $\epsilon_k = \hbar^2\, k^2/2m$ for the free particles. To analyze the equation of motion, we need to examine the commutator

$$[h_i, H] = \sum_k \epsilon_k [h_i,\ h_k^\dagger h_k]$$

$$= \sum_k \epsilon_k \left(\left[h_i, h_k^\dagger\right] h_k + h_k^\dagger [h_i, h_k] \right)$$

$$= \sum_k \delta_{ik} \epsilon_k h_k$$

$$= \epsilon_i h_i, \tag{S11}$$

which is simplified using the below commutator relations for fermions

$$\left[h_i, h_j^\dagger\right] = \delta_{ij}, \qquad \left[h_i, h_j\right] = \left[h_i^\dagger, h_j^\dagger\right] = 0. \tag{S12}$$

As a result, the equation of motion (S9) follows,

$$\omega G_{ij}^r(\omega) = \delta_{ij} + \epsilon_i G_{ij}^r(\omega), \tag{S13}$$

which yields

$$G_k^r(\omega) = \frac{1}{\omega + i0^+ - \epsilon_k}. \tag{S14}$$

The introduction of the converging factor $i0^+$ may seem arbitrary. To confirm the validity of this approach, let us perform the inverse Fourier transform

$$G_k^r(t) = \int_{-\infty}^{\infty} \frac{d\omega}{2\pi} \frac{e^{-i\omega t}}{\omega + i0^+ - \epsilon_k}. \tag{S15}$$

We aim to evaluate the integral with the Cauchy's residue theorem. When $t > 0$, the integration is closed in the contour of the lower half-plane, ensuring it encompasses the pole. Conversely, for $t < 0$, we have to close the contour in the upper half-plane. Since there are no poles in this upper half-plane, the integral vanishes. This analysis reveals that the causality is

consistent with the definition of retarded Green's function shown in (S6).

An important application is the perturbative system (Fermi-polaron problems), which states the presence of the impurity (excitons) in the Fermi sea. Following an approach proposed by Sidler *et al.*[20], the interacting Hamiltonian describing the system is

$$H = \sum_k \omega_{\mathrm{X}}(k) x_k^\dagger x_k + \sum_k \epsilon_k h_k^\dagger h_k + \sum_{k,k',q} V_q (x_{k+q}^\dagger h_{k'-q}^\dagger h_{k'} x_k + h.c.), \quad \text{(S16)}$$

$$\omega_{\mathrm{X}}(k) = \Delta E_{\mathrm{X}} + \frac{\hbar k^2}{2m_{\mathrm{exc}}} + \delta(E_{\mathrm{F}}), \epsilon_k = \frac{\hbar k^2}{2m_{\mathrm{h}}}, \quad \text{(S17)}$$

where x_k ($x_k^\dagger$) and h_k ($h_k^\dagger$) are the annihilation (creation) operators of an exciton and a hole respectively, while m_{exc} and m_{h} are the effective mass of the exciton and the hole. The interaction between the polarons mediated by the Fermi sea can be determined with the self-energy (Σ) which is the result of the variational method using Chevy Ansatz for the polaron state. This is given by

$$\Sigma(\omega) = \sum_q \left[\frac{1}{V} - \sum_{k=k_F}^{\Omega} \frac{1}{\omega + i0^+ - \omega_{\mathrm{X}}(q-k) + \epsilon(k) - \epsilon(q)}\right]^{-1}, \quad \text{(S18)}$$

where

$$\frac{1}{V} = \sum_{k=0}^{k_F} \frac{1}{\Delta E_{\mathrm{P}} - \omega_{\mathrm{X}}(0) + \omega_{\mathrm{X}}(k) + \epsilon(k)} \quad \text{(S19)}$$

with ΔE_{P} is the binding energy of the attractive polarons. By definition of the self-energy Σ, on one hand, we have the Dyson equation

$$G_k^r(\omega) = \frac{1}{\omega + i0^+ - \omega_{\mathrm{X}}(0) - \Sigma(\omega)}, \tag{S20}$$

with the impurity kinetic energy function $\omega_{\mathrm{X}}(0)$. On the other hand, we obtain the spectral function of the impurity excitons

$$A(\omega) = -\frac{1}{\pi}\mathrm{Im}G_k^r(\omega) = -\frac{1}{\pi}\mathrm{Im}[\omega + i0^+ - \omega_{\mathrm{X}}(0) - \Sigma(\omega)]^{-1}. \tag{S21}$$

In Supplementary Fig. 6, we observe distinct features in the simulation of the spectral function $A(\omega)$. First, one peak emerges at the trion resonance E_{T} with a slightly redshifted spectrum (attractive polarons), while another peak at the exciton energy (1.65 eV) is blueshifted with increasing Fermi energy (repulsive polarons). Furthermore, we observe a continuum of state with minimal oscillator strength which is identified as a molecular state, as proposed in the previous study[20].

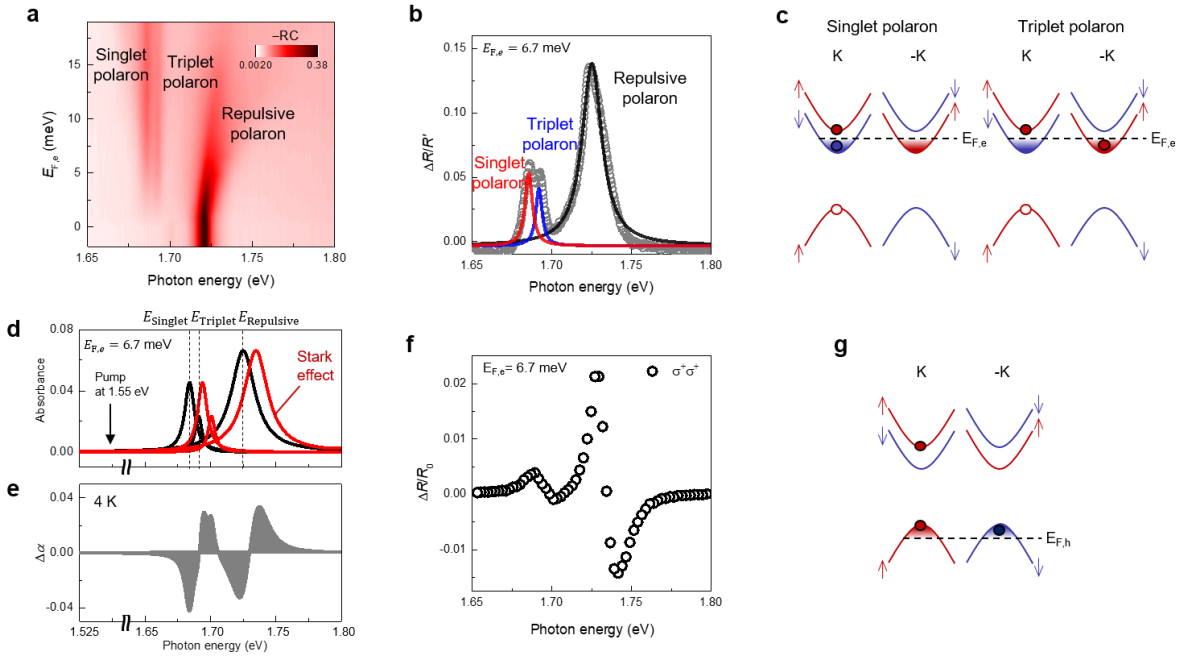

Supplementary Figure 1 | Reflectance contrast spectroscopy in an electron-doped regime. **a,** Reflectance contrast spectra $\Delta R/R'$ as a function of a photon energy (bottom axis) and Fermi energy $E_{\mathrm{F,e}}$ (left axis) in an electron-doped regime. Here, $\Delta R = R' - R$, where R is reflection signal from the WSe_2 monolayer sample and R' is reference spectrum from the background hBN nearby the sample. **b,** $\Delta R/R'$ when $E_{\mathrm{F,e}}$ is 6.7 meV. The gray circles represent the measured data. On top of the data, we show a sum of the fit functions for repulsive polarons (black line), singlet polarons (blue line) and triplet polarons (red line). **c,** Schematic illustration of the singlet and the triplet polaron configurations for WSe_2 where an exciton is formed in the K valley. Spin-up (-down) bands are shown in red (blue) color. Electrons in the spin-up (-down) state are represented by solid red (blue) circles and holes in the spin-up (-down) state are represented by empty red (blue) circles. **d,** Absorption spectra α when $E_{\mathrm{F,e}}$ is 6.7 meV without the 1.55-eV pump excitation (black lines). With the pump excitation (red lines), the Fermi polarons are blueshifted. **e,** The change of absorbance α is determined by subtracting the absorption spectra without the pump excitation (black lines in Supplementary Fig. 1d) from the spectra with the pump excitation (red lines in Supplementary Fig. 1d). **f,** The

differential reflectance spectrum $\Delta R/R_0$ measured at zero time-delay of the pump pulses when $E_{\mathrm{F,e}} =$ 6.7 meV. The pump and probe polarization is co-circularly polarized. Due to the overlap between two attractive polarons, it is very challenging to extract the shift of each attractive polaron resonance. **g,** Schematic illustration of the attractive polarons for WSe_2, where an exciton is formed in the K valley in the hole-doped regime.

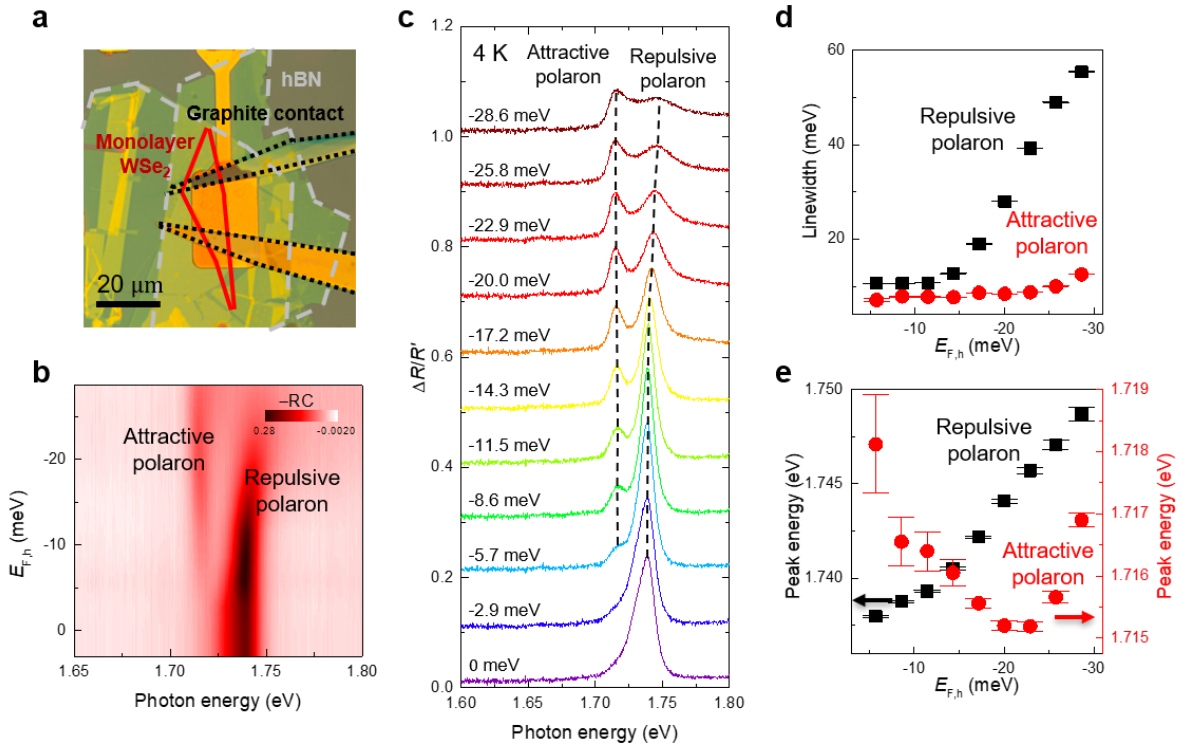

Supplementary Figure 2 | Spectra analysis of attractive and repulsive polarons in a hole-doped regime. a, An optical microscopic image of the hBN encapsulated WSe_2 device. This is different device from the device described in the main section. **b,** Reflectance contrast spectra $\Delta R/R'$ as a function of photon energy (bottom axis) and Fermi energy $E_{\mathrm{F,h}}$ (left axis). **c,** $\Delta R/R'$ spectra as a function of $E_{\mathrm{F,h}}$. The attractive polarons are redshifted and the repulsive polarons are blueshifted with increasing $E_{\mathrm{F,h}}$, i.e. more hole doping. The energy level and linewidth extracted from Supplementary Fig. 2c are plotted in **d** and **e**, respectively. **d,** The linewidths of both the attractive polarons (red circles) and the repulsive polarons (black squares) increase with $E_{\mathrm{F,h}}$. In contrast to the attractive polarons, an additional $E_{\mathrm{F,h}}$-dependent damping causes more broadened linewidth for the repulsive polarons. This arise because of the non-radiative transitions from the repulsive polarons to the attractive polarons. **e,** The repulsive polarons (black squares) exhibit a blueshift caused by the Pauli blocking effects and screening

effects due to the doped holes. The redshift feature of the attractive polarons (red circles) can be explained by the enhanced attractive interactions between the excitons and the itinerant holes. Vertical error bars in **d** and **e** are obtained from the fits.

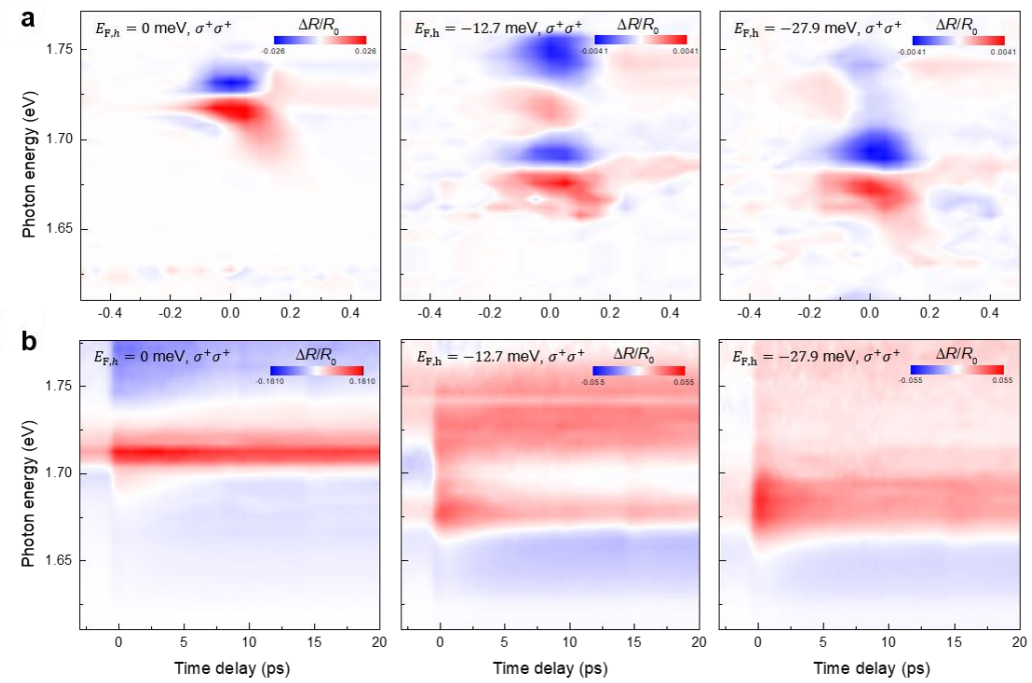

Supplementary Figure 3 | Ultrafast pump-probe spectroscopy under 3.1 eV pump excitation. a, Transient $\Delta R/R_0$ spectra when $E_{\mathrm{F,h}}$ is 0 meV (left), -12.7 meV (middle) and -27.9 meV (right). The σ^+-polarized pump (photon energy of 1.55 eV) is incident onto the sample shown in Supplementary Fig. 2a and the pump-induced $\Delta R/R_0$ changes are measured using with σ^+-polarized white-light pulse pulses. **b,** The pump-probe spectroscopy data with an above-gap pump of 3.1 eV when $E_{\mathrm{F,h}}$ is 0 meV (left), -12.7 meV (middle) and -27.9 meV (right) The decaying times of the pump-induced signals of both the attractive and the repulsive polarons decrease due to the scattering between the polarons and the carriers. Clearly, these data exhibit much longer relaxation dynamics compared to the data shown in **a**.

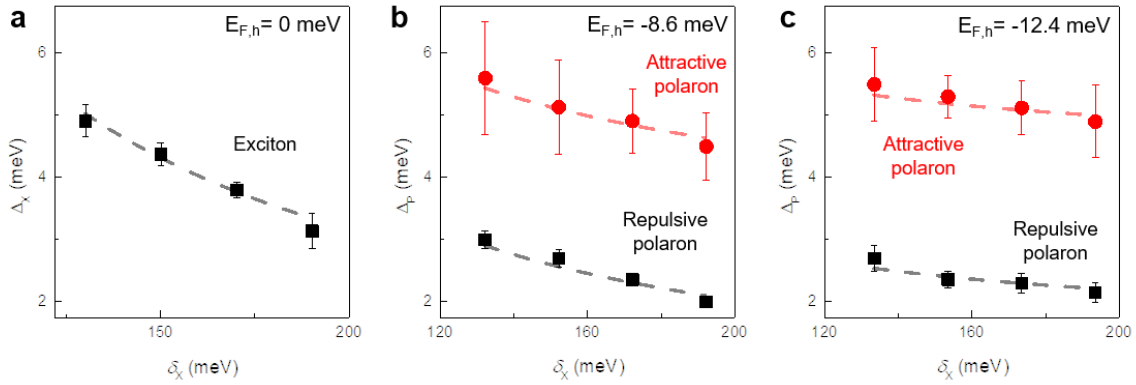

Supplementary Figure 4 | Pump detuning dependence for the shift of Fermi polarons. The shifts of excitons and Fermi polarons at $E_{\mathrm{F,h}} = 0$ (**a**), -8.6 (**b**), -12.4 meV (**c**) are shown as the functions of the pump detuning, δ_{X} is referenced to the repulsive polaron resonances. The gray dashed lines and red dashed lines represents the dependence of the pump detuning for the repulsive polarons and the attractive polarons, respectively. Vertical error bars in **a**, **b,** and **c** are obtained from the fits.

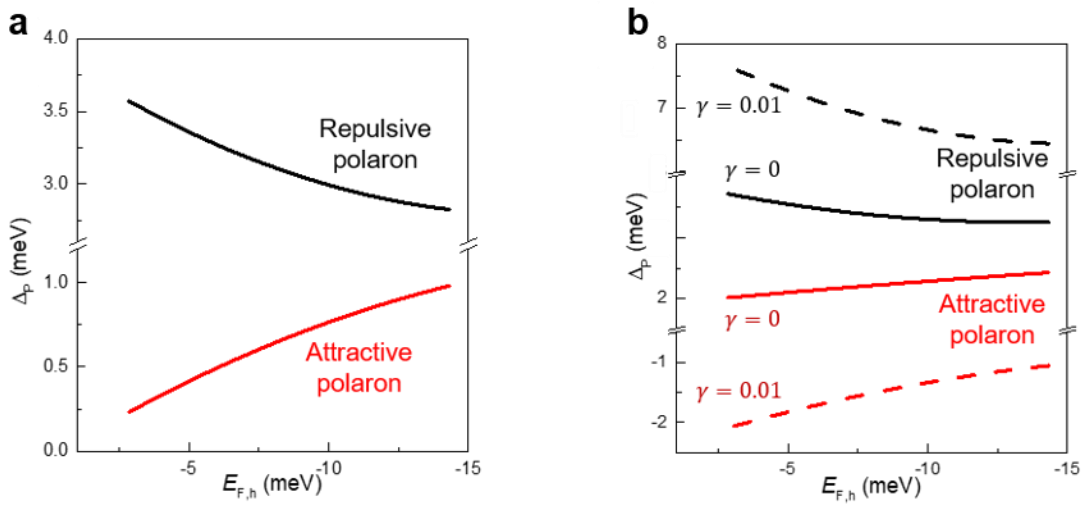

Supplementary Figure 5 | Isolated atom-photon interaction model. a, The energy shifts of the Fermi polarons calculated using the conventional atom-photon two-level model. When the dressed atom-photon model is used, Δ_P of attractive polarons is much smaller than that observed in the experimental data. The shift of attractive polarons (solid red line) increases, while that of repulsive polarons (solid black line) decreases. **b,** Δ_P computed using the three-level model with an interaction factor (γ). The solid line represents $\gamma = 0$ eV, indicating the absence of interaction between the Fermi polaron states, while the dashed line represents $\gamma = 0.01$ eV. When $\gamma = 0.01$ eV, the repulsive polaron experiences a larger shift due to the repulsion between the attractive and repulsive polaron states, the attractive polaron exhibits a red shift. Neither the results shown in **a** nor in **b** do not reproduce our measured data shown in Fig. 3c in the main text.

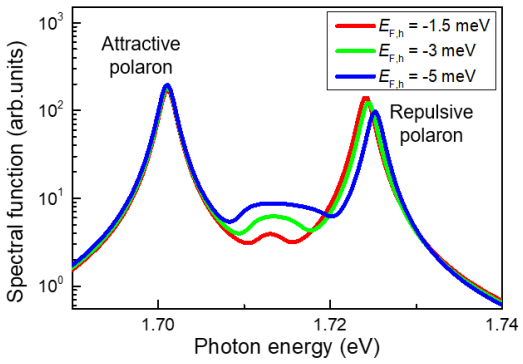

Supplementary Figure 6 | Gate-dependent spectral functions of Fermi polarons. The spectral function $A(\omega)$ is computed using the Chevy ansatz for three different values of $E_{\mathrm{F,h}}$: -1.5 meV (red), -3 meV (green) and -5 meV (blue). Note that the logarithmic scale of $A(\omega)$ is used to show the weak oscillator strength of the molecular state. With increasing $E_{\mathrm{F,h}}$ toward more hole doping, the attractive polarons shift slightly downwards (to the red) and the repulsive polarons shift upwards (to the blue).

References

1 Kośmider, K., González, J. W. & Fernández-Rossier, J. Large spin splitting in the conduction band of transition metal dichalcogenide monolayers. *Phys. Rev. B* **88**, 245636 (2013).

2 Plechinger, G. et al. Trion fine structure and coupled spin-valley dynamics in monolayer tungsten disulfide. *Nat. Commun.* **7**, 12715 (2016).

3 Yu, H., Liu, G. B., Gong, P., Xu, X. & Yao, W. Dirac cones and Dirac saddle points of bright excitons in monolayer transition metal dichalcogenides. *Nat. Commun.* **5**, 3876 (2014).

4 Efimkin, D. K., Laird, E. K., Levinsen, J., Parish, M. M. & MacDonald, A. H. Electron-exciton interactions in the exciton-polaron problem. *Phys. Rev. B* **103**, 075417 (2021).

5 Goldstein, T. et al. Ground and excited state exciton polarons in monolayer $MoSe_2$. *J. Chem. Phys.* **153**, 071101 (2020).

6 Siemens, M. E., Moody, G., Li, H., Bristow, A. D. & Cundiff, S. T. Resonance lineshapes in two dimensional Fourier transform spectroscopy. *Opt. Express* **18** (17), 17699-17708 (2010).

7 Huang, D. et al. Quantum dynamics of attractive and repulsive polarons in a doped $MoSe_2$,monolayer. *Phys. Rev. X* **13**, 011029 (2023).

8 Munkhbat, B. et al. Electrical control of hybrid monolayer tungsten disulfide-plasmonic nanoantenna light-matter states at cryogenic and room temperatures. *ACS Nano* **14**, 1196 (2020).

9 Chernikov, A. et al. Electrical tuning of exciton binding energies in monolayer WS_2. *Phys. Rev. Lett.* **115**, 126802 (2015)

10 Lin, T. N. et al. Many-body effects in doped WS_2 monolayer quantum disks at room temperature. *NPJ 2D Mater. Appl.* **3** (2019).

11 Liu, E. et al. Exciton-polaron Rydberg states in monolayer $MoSe_2$ and WSe_2. *Nat. Commun.* **12**, 6131 (2021)

12 Liu, E. et al. Gate tunable dark trions in monolayer WSe_2. *Phys. Rev. Lett.* **123**, 027401 (2019).

13 Sie, E. J. et al. Valley-selective optical Stark effect in monolayer WS_2. *Nat. Mater.* **14**, 290 (2015).

14 Kim, J. et al. Ultrafast generation of pseudo-magnetic field for valley exictons in WSe_2 monolayers. *Science* **346**, 1205 (2014).

15 Mondal, A. et al. Ultrafast exciton many-body interactions and hot-phonon bottleneck in colloidal cesium lead halide perovskite nanocrystals. *Phys. Rev. B* **98**, 115418 (2018).

16 Shrivastava, M. et al. Room-temperature anomalous coherent excitonic optical Stark effect in metal halide perovskite quantum dots. *Nano Lett.* **22**, 808 (2022).

17 Aneesh, J. et al. Ultrafast exciton dynamics in colloidal $CsPbBr_3$ perovskite nanocrystals: Biexciton effect and Auger recombination. *J. of Phys. Chem. C* **121**, 4734 (2017).

18 Cunningham, P. D., Hanbicki, A. T., Reinecke, T. L., McCreary, K. M. & Jonker, B. T. Resonant optical Stark effect in monolayer WS_2. *Nat. Commun.* **10**, 5539 (2019).

19 Fetter, A. L. & Walecka, J. D. *Quantum theory of many-particle systems*, (Dover Publications, 2003).

20 Sidler, M. et al. Fermi polaron-polaritons in charge-tunable atomically thin semiconductors. *Nat. Phys.* **13**, 255 (2017).